Design of distributed feedback cavity with controllable angular emission

Tianrui Zhai (翟天瑞), Xinping Zhang (张新平)*, Zhaoguang Pang (庞兆广), Hongmei Liu (刘红梅), and Baozeng Wang (王保增)

Institute of Information Photonics Technology and College of Applied Sciences, Beijing University of Technology, Beijing 100124, China

**Corresponding author: zhangxinping@bjut.edu.cn*

Received May 24, 2012; accepted July 10 2012; posted online November 13, 2012

The angular emission spectra of the distributed feedback (DFB) cavity are investigated theoretically and experimentally. An angular emission model of the relationship between the DFB cavity and its angular emission spectra is proposed. In the model, the DFB cavity can be decomposed into two parts: a grating and an active waveguide layer. So, the angular emission spectra of the DFB cavity are mainly determined by the period of the grating, the thickness of the waveguide and the material absorption during the feedback process. The theoretical model agrees well with the experimental results. It provides a convenient estimate for designing more efficient DFB polymer lasers and highly directional emission devices.

OCIS codes: 260.3160, 160.5470, 140.3490.

doi: 10.3788/COL201210.S22601.

In 1996, Tessler *et al*. demonstrated the first polymer laser[1], since then, great interests were attracted in designing various polymer lasers[2−6], developing multiple production techniques[7−10], and investigating the internal physical mechanisms[11−12]. However, the specific relationship between the emission parameters and the geometry of the distributed feedback (DFB) cavity has not been reported, which is important for both designing DFB lasers and enriching the theory of polymer lasers. In this letter, an analytical model for revealing the feedback mechanism of the polymer laser has been developed. In order to simplify the analysis, the DFB cavity can be decomposed into two parts: a grating and a waveguide, i.e., the waveguide grating structure. An active waveguide grating structure (AWGS) is employed to construct a DFB cavity, where a dielectric grating is fabricated on top of an active waveguide layer. So, the waveguide provides gain of the radiation and the grating provides feedback in combination with the waveguide.

The interaction between resonant modes of the waveguide and the grating is explored systematically using an analytical model, which is consistent with the experiments. The angular emission is mainly determined by the period of the grating, the thickness of the waveguide and the self absorption of the active material. The angle-resolved emission spectra reveal that a highly directional emission or a laser emission of DFB cavity requires: 1) the positive and negative first-order resonant must intersect; 2) the crossing spot must be within the gain spectra of the DFB cavity, which is determined by the absorption of the active material. So, the angular emission spectra can be quantitatively controlled by varying the parameters of the AWGS, which also provides practical guidelines for designing efficient DFB cavities.

The polymer employed in our experiment is a typical light-emitting conjugate poly [(9,9-dioctylfluorenyl-2,7-diyl)-alt-co- (1,4- benzo- {2,1',3}- thiadiazole)] (F8BT, the inset in Fig. 1(a)). The solution of F8BT in chloroform is spin-coated onto the glass substrate with an area of 20×20 mm^2 and a thickness of 1 mm to form the active waveguide. The absorption spectra peaked at about 470 nm and PL spectra centered on 550 nm are shown in Fig. 1(b). The grating structure on top of the polymer film is fabricated using interference lithography, which is written directly into the photoresist. A diode-pumped frequency-tripled (355 nm) solid-state laser with a pulse length of 500 ps and a repetition rate of 6.25 kHz is employed to perform the interference lithography and to pump the sample. The sample is mounted on a turret, and the angle-resolved emission spectrum is measured by an spectrometer (May a2000 PRD, Ocean Optics)(shown in Fig. 1(a)).

In the measurement, the axis of the detection head, the excitation laser beam, and the central axis of the turret should be across each other at the same point on the sample, as shown in Fig. 1(a). The laser spot at the crossing point has a diameter of about 3 mm. The distance between the detection head and the sample is about 10 cm. The above configuration ensures reliable measurements. The angle-resolved emission spectra of the AWGS device were recorded by scanning the angle α between the axis of the detection head and the normal of the AWGS device, as shown in Fig. 1(a). Meanwhile the angle β between the axis of the detection head and the excitation laser beam is fixed.

Figure 2 demonstrates how DFB is achieved in an AWGS device. Figure 2(a) shows the resonance modes of the AWGS device, where the propagation mode (beam A) of the waveguide cannot encounter its diffracted beam (beam B) by the grating in the reversed path, so no closed loop forms to provide feedback. Although beams A and B have an identical wavelength λ_{nr}, they propagate in different paths in the waveguide and are diffracted at different angles into air by the grating. However, in the homogeneous waveguide layer, each set of beams A and B has its "mirror-imaging" counterparts, which are symmetric about the normal of the substrate to form the colored ribbon, i.e., the sidelobe emission shown in Fig. 2(a). Since feedback is not supported by the scheme in Fig. 2(a), no lasing action is achieved in such an AWGS

 © 2012 Chinese Optics Letters

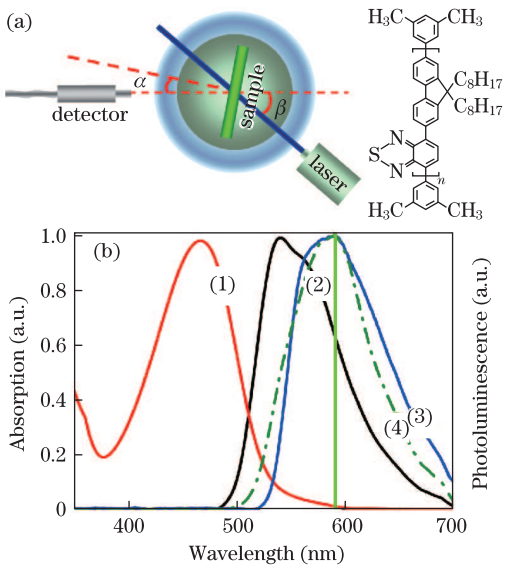

Fig. 1. (a) Schematic diagram of the experimental setup. The inset denotes the molecular formula of F8BT. (b) Absorption (1) and the photoluminescence (2) spectra of F8BT, the measured (3) and simulated (4) gain spectra of the AWGS.

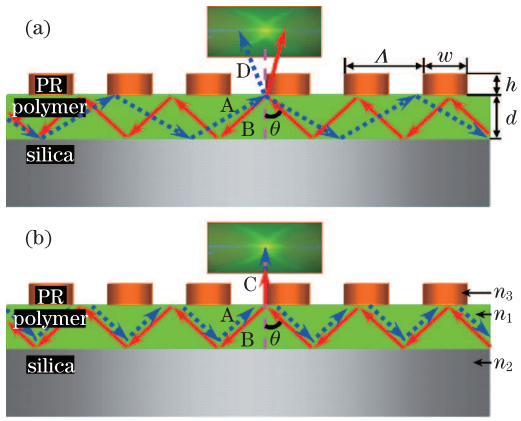

Fig. 2. Resonant mechanisms of the AWGS. (a) Schematic for sidelobe emission (no lasing); (b) schematic for surface emission (lasing). The upper panels are photos of surface-emitting colored ribbon of AWGS.

device. Therefore, the structural parameters have to be adjusted so that beams A and B reverse each other to form a closed loop. This defines a route for the design of a DFB laser. Figure 2(b) demonstrates schematically the resonance mode of a DFB cavity for a surface-emitting laser. In this case, beam B actually reverses the propagation path of beam A. Thus, a feedback loop forms to support possible lasing process. It can be seen that, for the resonance wavelength λ_r, the diffraction angles of the beams A and B are equal. So, there exists only one unified feedback loop forming by the two-order diffraction of the grating. Therefore, the first-order diffraction acts as the diffraction output which is vertical to the surface of the AWGS device as shown in Fig. 2(b). The energy in the resonant feedback loop is much higher than that shown in the Fig. 1(a), which enables the resonant wavelength more likely to lase or achieve highly directional emission.

The DFB mechanisms can be well explained by decomposing the AWGS cavity into two parts: a grating and a waveguide. The diffraction process of the grating can be described by

$$n_1 \Lambda \sin\theta + \Lambda \cos\psi = m_1 \lambda, \tag{1}$$

where n_1 is the refractive index of the waveguide as shown in Fig. 2(b); θ is the incident angle; ψ is the diffraction angle; m_1 is the order of diffraction (m_1=0, ±1, ±2,$\cdots$). And the resonant mode in the waveguide layer is determined by the condition of the guided mode

$$k_0 d n_1 \cos\theta - \varphi_1 - \varphi_2 = 2m_2\pi, \tag{2}$$

where the first item of Eq. (2) is the phase shift of the beam passing through the waveguide; k_0 is the wave vector in the vacuum; φ_1 and φ_2 are the total reflection phase shift of the upper and the lower interface of the waveguide, respectively; m_2 is the mode number (m_2=0, 1, 2,$\cdots$). Considering all the resonant phenomenons in the DFB cavity are within the visible spectra in our experiment, m_1 and m_2 are assigned to 1 and 0, respectively. Meanwhile, combining Eqs. (1) and (2), all the phenomenon in AWGS device can be depicted by the analytical model:

$$\lambda = \Lambda\left[\cos\psi + \sqrt{1-(\Phi/k_0 d)^2}\right], \tag{3}$$

where Φ=ϕ_1+ϕ_2. So, it can be seen that the emission wavelength λ is approximately proportional to the cosine of the diffraction angle ψ. It is also worth noting that the actual emission spectrum of the AWGS device, i.e., the gain spectrum of the cavity, is some red shift (about 50 nm in our experiment) compared with the photoluminescence (PL) spectra of F8BT (shown in line 2, 4 in Fig. 1(b)). It can be explained by considering an absorption model as

$$I_{\text{gain}} = I_{\text{PL}} \frac{1-10^{-NI_{\text{abs}}}}{1-10^{-I_{\text{abs}}}}, \tag{4}$$

where I_{gain}, I_{PL}, I_{abs} are the gain spectra of the cavity, the PL and absorption spectra of F8BT, respectively. Actually, a diffraction beam A or B will be reflected N times in the active waveguide before exit, then the beam will encounter N times absorption and amplification of F8BT simultaneously. So the frontier of the PL spectra will be decreased and the posterior of the PL spectra will be uplifted, forming the final gain spectra of the DFB laser cavity. The dotted line (4) shown in Fig. 1(b) is the simulated gain spectrum of the cavity by considering N=20.

The angle-resolved emission spectroscopy is systematically investigated to find the effects of AWGS device parameters using the analytical model.

Figure 3 shows the simulated angular emission spectra dependent on the period of the grating. It can be seen that the positive and negative first-order resonant mode overlap each other in a certain period range, which is about between 320–520 nm determined by the gain spectra of the AWGS cavity. Theoretical simulations and experimental results show that the wavelength of the crossing spot increases 1 nm when the period of the grating increases 1 nm.

It should be noted that the wavelength of the crossing

spot should be within the gain spectra of the DFB cavity to achieve lasing. It has been reported that F8BT can lase at 591 nm[13] which is far from the center of the PL spectra but around the center of the gain spectra of the laser cavity (the green line in Fig. 1(b)). This phenomenon can be well explained by the absorption model.

Figure 4 shows that the wavelength of the crossing spot can also be fine tuning by varying the thickness of the active waveguide. When the thickness of the waveguide increases 1 nm, the wavelength of the crossing spot increases 0.125 nm. The simulated results (the left panels in Fig. 4) are in good agreement with the corresponding

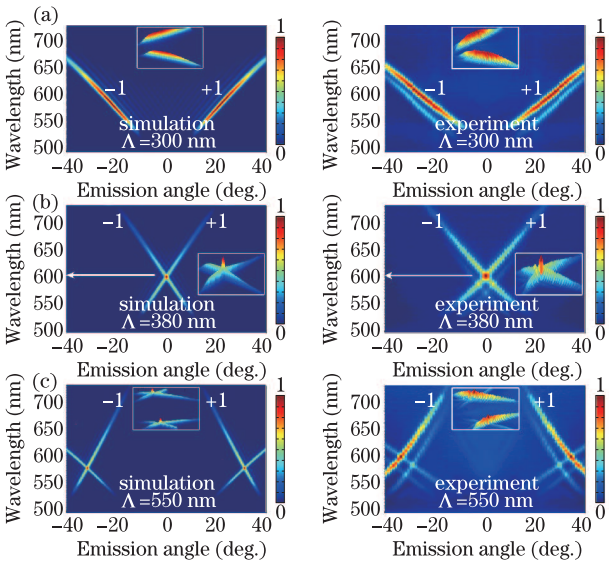

Fig. 3. Angular emission spectra of AWGS with different grating periods Λ of (a) 300 nm; (b) 380 nm; (c) 550 nm. $d \approx 200$ nm, $h \approx 80$ nm, $w \approx 140$ nm. The left/right panels are the simulated/experimental results. The insets are the three-dimensional perspective of the angular emission spectra.

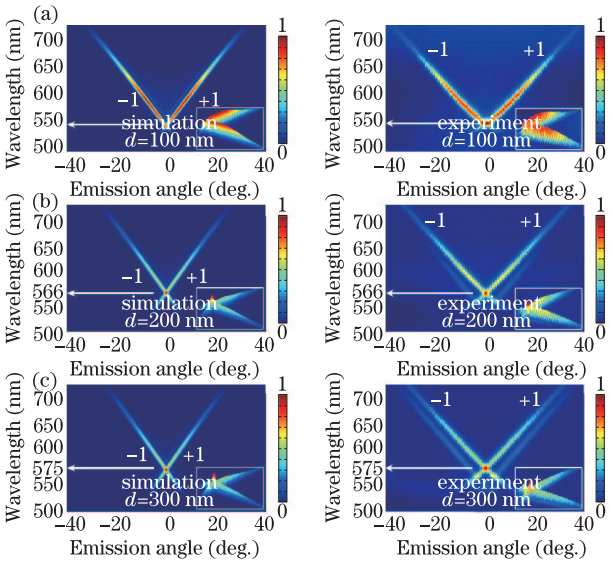

Fig. 4. Angular emission spectra of AWGS with different waveguide thicknesses h of (a) 100 nm; (b) 200 nm; (c) 300 nm. $\Lambda \approx 350$ nm, $h \approx 80$ nm, $w \approx 140$ nm. The left/right panels are the simulated/experimental results. The insets are the three-dimensional perspective of the angular emission spectra.

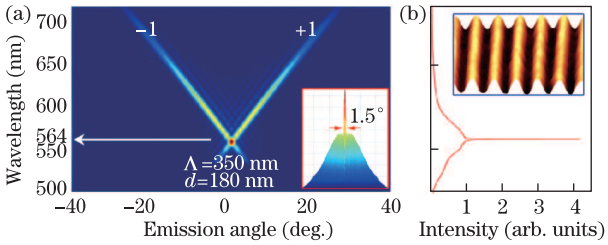

Fig. 5. (a) Simulated angle-resolved emission spectra of an AWGS device and (b) its laser emission spectra. $h \approx 80$ nm. The inset in (a) is the side view of the angular emission spectra (no lasing). The inset in (b) is the AFM image of the AWGS device.

experimental results (the right panels in Fig. 4). According to Eq. (2), the increase of the thickness d leads to a larger incident angle θ. And considering Eq. (1), a larger θ will produce a longer resonance wavelength.

The dependence of angle-resolved emission spectra on duty cycle of the grating structures is also studied. It is found that the variation of the duty cycle of the grating structure only has a very weak effect on the position of the resonance wavelength.

Considering the optimized period of the grating and the optimized thickness of the waveguide, an AWGS cavity with a period of 350 nm and a thickness of 200 nm are designed to obtain lasing. Figure 5(a) shows the simulated angular emission spectra of the AWGS, and Fig. 5(b) shows the corresponding experimental laser emission spectra. The laser emission is centered at 564 nm with a linewidth of about 0.4 nm at full width at half maximum (FWHM), which is precisely the resonant wavelength as our model predicted. Additionally, the half divergence angle of the resonant peak of the crossing spot is typically smaller than 1° (the inset in Fig. 5(a)), which can be used as a highly directional emission device.

In conclusion, the theoretical model shows that the angle-resolved emission spectra of a DFB cavity based on AWGS can be controlled by varying the period and the thickness of the active waveguide, which is in good agreement with the experiment results. It provides an efficient method for designing the DFB polymer lasers and highly directional emission devices.

The authors acknowledge the National Natural Science Foundation of China (Nos. 11074018 and 11104007), the Doctoral Program of Higher Education of China (No. RFDP 20091103110012), and the Beijing Educational Commission (No. KM201210005034) and the Natural science foundation of Hebei Province (No. A2012205085) for the financial support.

References

1. N. Tessler, G. Denton, and R. Friend, Nature **382,** 695 (1996).
2. C. Bauer, H. Giessen, B. Schnabel, E. Kley, C. Schmitt, U. Scherf, and R. Mahrt, Adv. Mater. **13,** 1161 (2001).
3. J. Stehr, J. Crewett, F. Schindler, R. Sperling, G. von Plessen, U. Lemmer, J. Lupton, T. Klar, J. Feldmann, and A. Holleitner, Adv. Mater. **15,** 1726 (2003).
4. B. Wenger, N. Tétreault, M. Welland, and R. Friend, Appl. Phys. Lett. **97,** 193303 (2010).

5. T. Zhai, X. Zhang, and Z. Pang, Opt. Express **19,** 6487 (2011).
6. T. Zhai, X. Zhang, Z. Pang, X. Su, H. Liu, S. Feng, and L. Wang, Nano Lett. **11,** 4295 (2011).
7. M. Gaal, C. Gadermaier, H. Plank, E. Moderegger, A. Pogantsch, G. Leising, and E. List, Adv. Mater. **15,** 1165 (2003).
8. D. Pisignano, L. Persano, R. Cingolani, G. Gigli, F. Babudri, G. Farinola, and F. Naso, Appl. Phys. Lett. **84,** 1365 (2004).
9. E. Namdas, M. Tong, P. Ledochowitsch, S. Mednick, J. Yuen, D. Moses, and A. Heeger, Adv. Mater. **21,** 799 (2009).
10. T. Zhai, X. Zhang, Z. Pang, and F. Dou, Adv. Mater. **23,** 1860 (2011).
11. H. Kogelnik and C. Shank, J. Appl. Phys. **43,** 2327 (1972).
12. G. Heliotis, R. Xia, G. Turnbull, P. Andrew, W. Barnes, I. Samuel, and D. Bradley, Adv. Funct. Mater. **14,** 91 (2004).
13. R. Xia, G. Heliotis, P. Stavrinou, and D. Bradley, Appl. Phys. Lett. **87,** 031104 (2005).